DIRECT NUMERICAL SIMULATIONS OF FLOW BOILING IN MICROCHANNELS

Federico Municchi[1], Hannah R. Moran[2], Ismail El Mellas[3], Omar K. Matar[2], Mirco Magnini[3*]

[1]Colorado School of Mines, 1500 Illinois St., Golden, CO 80401
[2]Chemical Engineering Department, Imperial College London, London SW7 2AZ, UK
[3]Dept. of Mechanical, Materials and Manufacturing Engineering, University of Nottingham, Nottingham NG7 2RD, UK

ABSTRACT

Flow boiling within multi-microchannel evaporators represents a compact and efficient solution to dissipate high heat fluxes from small surface areas, such as those generated by computer microchips, laser diodes, batteries or fuel cells. Our fundamental knowledge of the underlying flow and heat transfer mechanisms has advanced greatly in the past decades, nonetheless there is still general disagreement on the best microchannel design that can maximise heat transfer given the heat load and geometrical constraints. In this work, we present an application of the geometric Volume-of-Fluid solver available in OpenFOAM to simulate flow boiling in multi-microchannel evaporators. The focus of the study is on the single microchannel unit, which is modelled accounting also for the base and lateral walls in order to assess conjugate heat transfer effects. The numerical model also incorporates a phase change model based on the kinetic theory of gases, superior surface tension estimation based on smoothing and redistribution of the surface force, and a sub-grid evaporation microlayer to capture the contact line heat transfer. We first study the flow of elongated bubbles in square and rectangular microchannels in adiabatic conditions to assess the impact of the channel shape on the topography of the lubrication film, and then we present the results of flow boiling simulations in microchannels of different aspect ratio and thickness of the lateral walls.

1. INTRODUCTION

While the recent advances in manufacturing technology enabled mass production of devices operating at high power densities (e.g., microelectronics, batteries, miniature fuel cells, etc.), they also led to a dramatic surge in the pressure for developing efficient cooling systems. Since such high-power devices tend to produce heat fluxes on the order of several MW/m^2, they require a heat-removal capability beyond that of traditional single phase cooling systems, which is generally bounded to less than 1 MW/m^2 [1]. On the contrary, multiphase flows with phase-change represent a viable technological solution, since additional energy can be dissipated in the form of latent heat. Within microchannels, the growing bubbles quickly occupy the entire channel cross-section such that slug and annular flows are the most common flow patterns, owing to the dominant effect of surface tension forces which rearrange the liquid phase into a thin lubricating film surrounding the long bubbles or high-speed gas core. When the flow pattern is characterised by thin liquid films, it is generally accepted that the heat transfer is inversely proportional to the thickness of this film, as the main heat transfer mechanism between the hot channel wall and the liquid-vapour interface is one-dimensional heat conduction across the film. Therefore, the distribution and thickness of the film play a key role in microchannel heat transfer [2]. Despite the large number of experimental studies conducted on boiling heat transfer in microchannels, there is still general disagreement on the underlying dynamics, because the existing experimental techniques cannot yet access the small spatial and temporal scales of the flow with sufficient resolution. This resulted into a lack of clarity about the best channel design to optimise heat transfer. Multichannel evaporators are usually nonuniformly heated, with the heat load being applied through the bottom, base wall. Fu et al. [3] performed a systematic analysis of the channel aspect ratio, here defined as width-to-height $\epsilon = W/H$, for $\epsilon = 0.17 - 1.2$ and concluded that the best heat transfer was achieved with the square channel, while performances deteriorated when $\epsilon < 1$. Markal et al. [4] tested aspect-ratios in the range $\epsilon = 0.37 - 5$ and observed that the heat transfer coefficient increased

monotonically with ϵ. Al-Zaidi et al. [5] tested channel aspect-ratios $\epsilon = 0.5 - 2$ and reported higher heat transfer coefficients when $\epsilon = 2$. Magnini and Matar [2] performed a numerical study for uniformly heated noncircular channels in the range $\epsilon = 1 - 8$ and highlighted that the performance depended on the liquid film distribution, with $\epsilon = 1$ performing best at low flow rates owing to the very thin films established in square channels, while larger aspect ratios performing best at higher flow rates where the film in square channels became very thick; however, their study was done at low values of heat flux and the liquid film did never dry. The objective of the present work is to extend the numerical study of Magnini and Matar [2] to cover higher heat fluxes, up to $q = 100 \, kW/m^2$, and account for bubble nucleation, film dryout, contact line dynamics and conjugate heat transfer across the microchannel walls. We first present the results of a systematic analysis of the geometrical features of the liquid film around long bubbles in adiabatic flow conditions in microchannels of $\epsilon = 1 - 8$. Afterwards, we present a systematic analysis of the flow and heat transfer features for flow boiling in microchannels of different aspect ratios and thicknesses of the lateral walls of the channel.

2.   METHODOLOGY

We employ a self-developed version of the Volume-of-Fluid (VoF) solver available in the opensource simulation package ESI-OpenFOAM v. 2106. These solve the unsteady governing equations for an incompressible flow, namely volume fraction, mass, momentum and energy conservation:

$$\frac{\partial \alpha}{\partial t} + \nabla \cdot (\alpha \boldsymbol{u}) = \frac{1}{\rho_v} m_i'' |\nabla \alpha|, \tag{1}$$

$$\nabla \cdot \boldsymbol{u} = \left(\frac{1}{\rho_v} - \frac{1}{\rho_l} \right) m_i'' |\nabla \alpha|, \tag{2}$$

$$\frac{\partial (\rho \boldsymbol{u})}{\partial t} + \nabla \cdot (\rho \boldsymbol{u}\boldsymbol{u}) = -\nabla p + \nabla \cdot [\mu (\nabla \boldsymbol{u} + \nabla \boldsymbol{u}^T)] + \boldsymbol{F_\sigma}, \tag{3}$$

$$\frac{\partial (\rho c_p T)}{\partial t} + \nabla \cdot (\rho c_p \boldsymbol{u} T) = \nabla \cdot (\lambda \nabla T) - m_i'' [h_{lv} - (c_{p,v} - c_{p,l})T] |\nabla \alpha|, \tag{4}$$

where α indicates the VoF fraction ($\alpha = 1$ in the vapor), t the time, $\boldsymbol{u}$ the fluid velocity vector, ρ the density, m_i'' the evaporation mass transfer, p the pressure, μ the dynamic viscosity, $\boldsymbol{F_\sigma}$ the surface tension force, c_p the specific heat, T the temperature, λ the thermal conductivity, and h_{lv} the latent heat. The subscripts l and v refer to the liquid and vapor specific properties, respectively. Equation (1) is solved using a geometric VoF method as implemented in OpenFOAM's solver isoAdvector. The surface tension force is calculated as a volume force as $\boldsymbol{F_\sigma} = \hat{\rho} \sigma \kappa \nabla \alpha$, where $\hat{\rho} = 2\rho/(\rho_l + \rho_v)$ redistributes the force to the heavier phase to reduce spurious velocities, σ is the surface tension coefficient and κ is the interface curvature, here evaluated via gradients of a smoothed version of the volume fraction. The evaporation mass transfer is calculated based on the local temperature field according to the Hertz-Knudsen-Schrage relationship [2], $m_i'' = (T - T_{sat})/(h_{lv}R_i)$ where R_i is the interfacial resistance to heat transfer and T_{sat} the saturation temperature. An extra evaporation source term is added to the computational cells at the heated walls cut by the interface, to account for the presence of an evaporation microlayer which is too small to be captured by the mesh. The evaporation microlayer dynamics is governed by a one-dimensional partial differential equation where the microlayer thickness h depends on time and wall-parallel coordinate x and its dynamic results from the balance of the flows induced by evaporation, surface tension and disjoining pressures, according to the following equation which has been taken from Ajaev et al. [6]:

$$\frac{\partial h}{\partial t} + \frac{\partial Q}{\partial x} + E = 0, \tag{5}$$

$$Q = \frac{h^3}{3\mu_l}\frac{\partial p_l}{\partial x}, \qquad p_l = p_v - \sigma\kappa - \frac{A}{h^3}, \qquad E = \frac{T_w - T_{sat}(1 + \Delta p/\rho_l h_{lv})}{\rho_l h_{lv}(h/\lambda_l + R_i)}, \tag{6}$$

where Q is the film flow rate, E is the film evaporation rate, A is the dispersion coefficient, T_w is the wall temperature and $\Delta p = p_v - p_l$. The equations above are solved in Matlab for a range of wall temperatures and the evaporation rate integrated along the evaporating microlayer is added as an extra source to Eqs. (1), (2) and (4). To avoid calculating the mass source twice in these cells, the contribution from the Hertz-Schrage-Knudsen model is locally switched off. The numerical model is complemented by the solution of the unsteady heat conduction equations across the solid walls, where the temperature field is coupled with the fluidic zones to match temperature and heat flux at the matching boundaries.

3. RESULTS

We model the flow of long bubbles in noncircular channels in isothermal conditions to study the perimetral distribution of the liquid film. We consider aspect ratios $\epsilon = 1 - 8$, bubble capillary numbers from $Ca_b = \mu_l U_b/\sigma = 0.005$ to $Ca_b = 1$, and Weber numbers from $We_b = \rho_l U_b^2 D_h/\sigma \ll 1$ to $We_b = 100$, with U_b being the bubble speed and D_h the hydraulic diameter of the channel. The hydraulic diameter is the same for all aspect-ratios. Figure 1(a) displays the bubble width as a function of the bubble speed for the visco-capillary regime ($We_b < 1$), and compare the results with those achieved by Lózar et al. [7], used as a benchmark. The bubble width is always measured $1.96W$ behind the bubble nose. It can be seen that the bubble width, when normalised with the channel width, decreases with increasing the capillary number and the channel aspect ratio, such that a thicker liquid film is left upon the side walls. The situation reverses at small capillary numbers, where larger aspect-ratios tend to generate much thinner films once that the interface profile forms a dimple over the side wall. This is observed for $\epsilon = 2$ when $Ca_b < 0.01$, while it happens at much smaller capillary numbers for higher aspect-ratio channels. Not reported in the figure, we have also measured the thickness of the liquid film left upon the horizontal walls and we observe that this is always thinner than that left upon the short lateral wall, and it obeys a scaling law which is independent of the aspect ratio provided that the hydraulic radius of the channel is the same.

In our second work we study the dynamics of a vapour bubble nucleating at the wall of a heated microchannel. We emulated the experimental conditions of Mukherjee et al. [8] as a validation test. The
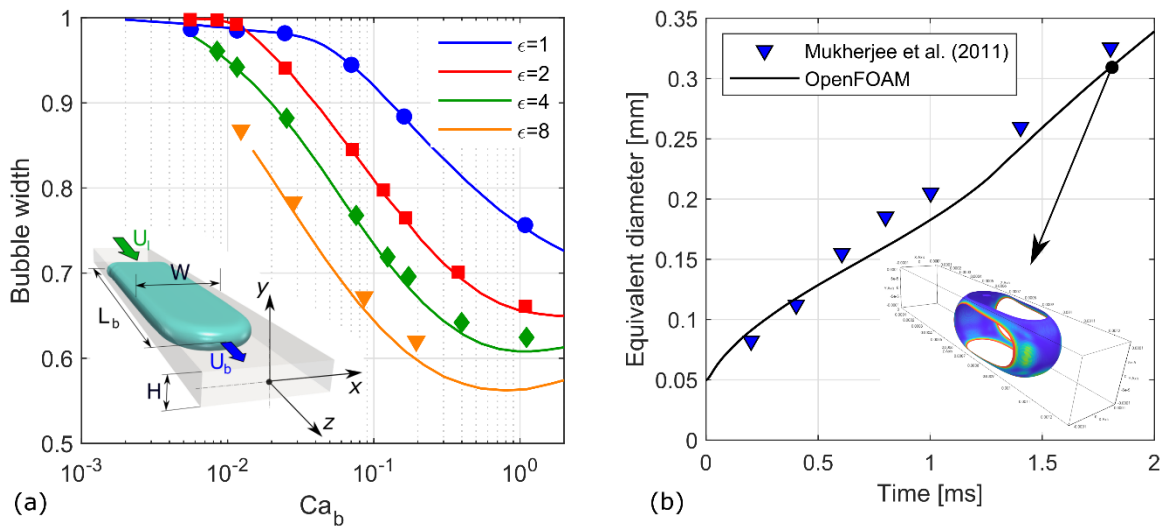
Fig. 1: (a) Bubble width, normalised by the channel width, in isothermal flow. Comparison between (solid lines) numerical results of de Lózar et al. [7] and our results (symbols). (b) Bubble growth from boiling in a 229 mm square microchannel. Comparison of experimental data of Mukherjee et al. [8] and our results. The inset in (b) shows a snapshot of the bubble profile after 1.8 ms, coloured with the local evaporation rate, with the empty regions within the bubble identifying dry vapour regions.
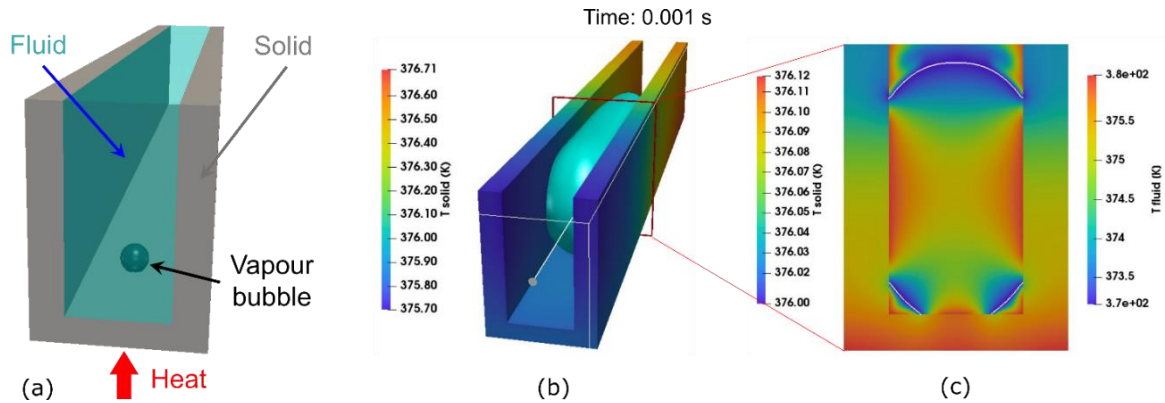
Fig. 2: (a) Simulation setup for conjugate heat transfer analyses. (b) Snapshot of the bubble (in light blue) and temperature distribution in the walls and (c) temperature fields within fluid and walls on a cross-section extracted from (b).

fluid is water, that boils at 1 atm at $T_{sat} = 100$ ℃. Water enters in saturated conditions in a square microchannel of size 229 μm, where the bottom and side walls are maintained at a temperature of 102.1 ℃; the top wall is adiabatic. The mass flux of water is $G = 123$ kg/m^{2}s. We initialise a small spherical bubble of initial diameter 50 μm and hydrophilic contact angle 30° at the bottom wall at $t = 0$, together with a steady-state temperature profile obtained with a preliminary liquid-only simulation. The comparison of numerical and experimental results in terms of equivalent diameter of the bubble vs time is provided in Fig. 1(b). The bubble undergoes an initial fast growth due to the initial superheated liquid surrounding it, after which the evaporation rate becomes rather constant while the bubble grows spherically. As the bubble begins elongating after about 1 ms, the evaporation rate slightly increases but then settles again once dry patches begin forming at the wall. The same bubble dynamics have been observed by Mukherjee et al. [8], and our results match theirs remarkably well. The inset in Fig. 1(b) shows that after 1.8 ms, extended dry vapour patches cover all the four microchannel walls. The bubble surface in Fig. 1(b) is coloured with the local evaporation rate, and it can be seen that the largest evaporation rate is detected along the triple solid-liquid-vapour contact line, where the temperature is the highest. Then, we have performed a series of studies by adding copper base and lateral walls as indicated in Fig. 2(a), testing different channel aspect-ratios and lateral wall thicknesses for constant hydraulic diameter, and applying a base heat flux of 100 kW/m^2. Figure 2 shows configuration and a snapshot of the results obtained with $\epsilon = 0.5$ and lateral fins of width 0.07 mm. It can be seen in Fig. 2(c) that the high heat transfer induced by the contact line is very effective in cooling down the internal surface of the walls, while the thermal inertia of the walls tends to dampen this effect when observed from the outside surface.

4.   CONCLUSIONS

We have studied the dynamics of bubbles in a microchannel first in adiabatic and then in flow boiling conditions. The adiabatic study emphasises that higher aspect-ratio channels induce thick liquid films over the short wall, whereas the film upon the longer wall is independent of the aspect-ratio. The temperature fields for flow boiling in microchannels show that contact lines are very effective in cooling down the walls; the planned systematic analysis of the impact of channel aspect-ratio and wall thickness promises to shed light on the best design of multichannel evaporators.

ACKNOWLEDGEMENTS

REFERENCES

[1]   T. G. Karayiannis, M. M. Mahmoud, "Flow boiling in microchannels: Fundamentals and applications", Appl. Therm. Eng., vol. 115, pp. 1372-1397, 2017.

[2]   M. Magnini, O. K. Matar, "Numerical study of the impact of the channel shape on microchannel boiling heat transfer", Int J. Heat & Mass Transfer, vol. 150, n. 119322, 2020.

[3]   B.-R. Fu, C.-Y. Lee, C. Pan, "The effect of aspect ratio on flow boiling heat transfer of HFE-7100 in a microchannel heat sink", Int J. Heat & Mass Transfer, vol. 58, pp. 53-61, 2013.

[4]   B. Markal, O. Aydin, M. Avci, "Effect of aspect ratio on saturated flow boiling in microchannels", Int J. Heat & Mass Transfer, vol. 93, pp. 130-143, 2016.

[5]   A. H. Al-Zaidi, M. M. Mahmoud, T. G. Karayiannis, "Effect of aspect ratio on flow boiling characteristics in microchannels", Int J. Heat & Mass Transfer, vol. 164, n. 120587, 2021.

[6]   V. S. Ajaev, Interfacial Fluid Mechanics, Springer, 2012.

[7]   A. de Lózar, A. Juel, A. L. Hazel, "The steady propagation of an air finger into a rectangular tube", J. Fluid Mech., vol. 614, pp. 173-195, 2008.

[8]   A. Mukherjee, S. G. Kandlikar, Z. J. Edel, "Numerical study of bubble growth and wall heat transfer during flow boiling in a microchannel", Int J. Heat & Mass Transfer, vol. 54, pp. 3702-3718, 2011.